UC Berkeley
UC Berkeley Previously Published Works

Title
Influence of Molecular Structure and Chemical Functionality on the Heterogeneous OH-Initiated Oxidation of Unsaturated Organic Particles

Permalink
https://escholarship.org/uc/item/0cv5595k

Journal
The Journal of Physical Chemistry A, 118(23)

ISSN
1089-5639

Authors
Nah, Theodora
Kessler, Sean H
Daumit, Kelly E
et al.

Publication Date
2014-06-12

DOI
10.1021/jp502666g

Peer reviewed

Influence of Molecular Structure and Chemical Functionality on the Heterogeneous OH-Initiated Oxidation of Unsaturated Organic Particles

Theodora Nah,[†,‡] Sean H. Kessler,[§] Kelly E. Daumit,[∥] Jesse H. Kroll,[§,∥] Stephen R. Leone,[†,‡,⊥] and Kevin R. Wilson*,[‡]

[†]Department of Chemistry, University of California, Berkeley, California 94720, United States

[‡]Chemical Sciences Division, Lawrence Berkeley National Laboratory, Berkeley, California 94720, United States

[§]Department of Chemical Engineering, Massachusetts Institute of Technology, Cambridge, Massachusetts 02139, United States

[∥]Department of Civil and Environmental Engineering, Massachusetts Institute of Technology, Cambridge, Massachusetts 02139, United States

[⊥]Department of Physics, University of California, Berkeley, California 94720, United States

ABSTRACT: The kinetics and products of the heterogeneous OH-initiated oxidation of squalene ($C_{30}H_{50}$, a branched alkene with 6 C=C double bonds) particles are measured. These results are compared to previous measurements of the OH-initiated oxidation of linoleic acid ($C_{18}H_{32}O_2$, a linear carboxylic acid with 2 C=C double bonds) particles to understand how molecular structure and chemical functionality influence reaction rates and mechanisms. In a 10% mixture of O_2 in N_2 in the flow reactor, the effective uptake coefficients (γ_{eff}) for squalene and linoleic acid are larger than unity, providing clear evidence for particle-phase secondary chain chemistry. γ_{eff} for squalene is 2.34 ± 0.07, which is smaller than γ_{eff} for linoleic acid (3.75 ± 0.18) despite the larger number of C=C double bonds in squalene. γ_{eff} for squalene increases with $[O_2]$ in the reactor, whereas γ_{eff} for linoleic acid decreases with increasing $[O_2]$. This suggests that the chain cycling mechanism in these two systems is different since O_2 promotes chain propagation in the OH + squalene reaction but promotes chain termination in the OH + linoleic acid reaction. Elemental analysis of squalene aerosol shows that an average of 1.06 ± 0.12 O atoms are added per reactive loss of squalene prior to the onset of particle volatilization. O_2 promotes particle volatilization in the OH + squalene reaction, suggesting that fragmentation reactions are important when O_2 is present in the OH oxidation of branched unsaturated organic aerosol. In contrast, O_2 does not influence the rate of particle volatilization in the OH + linoleic acid reaction. This indicates that O_2 does not alter the relative importance of fragmentation reactions in the OH oxidation of linear unsaturated organic aerosol.
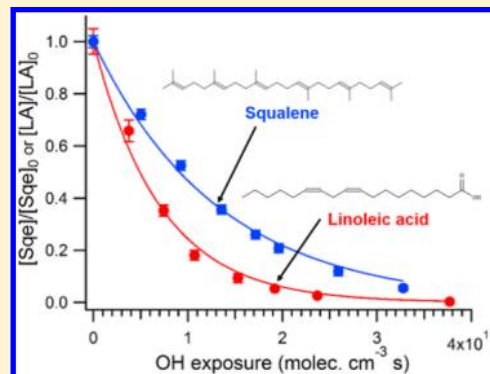
1. INTRODUCTION

Sub-micrometer organic particles play key roles in atmospheric and combustion chemistry. Once airborne, organic particles can undergo multiple oxidation reactions (i.e., multigenerational oxidation) with gas-phase oxidants such as hydroxyl (OH) radicals, chlorine (Cl) atoms and ozone (O_3)[1−3] to alter the physicochemical properties of the particles.[4−6] The OH radical is an important oxidant in many environmental and combustion processes.[1] Despite ongoing efforts to better understand the underlying reaction mechanisms in the OH-initiated oxidation of organic particles, much more is known about the reaction rates and mechanisms of homogeneous reactions between gas-phase organic compounds and OH radicals.[7−10] The vast amount of experimental data for different gas-phase reactions has enabled the formulation of general rules for predicting the reactivity of a molecule based on its molecular structure. These rules, summarized as structure activity relationships (SARs),[11,12] provide estimates for rate coefficients of gas-

phase oxidation reactions. As a starting point, the heterogeneous oxidation of organic particles is typically considered within the context of known gas-phase reaction mechanisms and SARs, in an effort to ascertain key similarities and differences between heterogeneous and homogeneous oxidation reactions.

Moise et al.[13] showed that many types of chemical reactions that are slow in the gas phase ($k < 10^{-14}$ molec^{-1} cm^3 s^{-1}) are enhanced by several orders of magnitude (10 to 10^4) when they occur at an organic surface. Liu et al.[14] observed that the heterogeneous reaction of squalane particles with Cl atoms is only 2 times faster than with OH radicals. This is in contrast to gas-phase SAR estimates, which predict that the Cl + squalane reaction would occur 32 times faster than the OH + squalane

reaction. These discrepancies in the reaction rates can be explained by the chemical differences between a gas−particle interface and a homogeneous gas-phase environment. In the gas phase, reaction rates and product branching ratios depend on the molecular structure, transition states and reaction pathways available for the radical intermediates. In heterogeneous reactions, interfacial molecular orientation and thermodynamic phase may play a larger role in controlling reaction rates and product branching ratios.[15] Additional complexity arises when there are particle-phase secondary chain reactions that accelerate the overall reactivity of the organic particle. Hence predictions of heterogeneous reaction rates and mechanisms based exclusively on the molecular structure (e.g., the number and type of reactive sites in an isolated molecule) may often be incomplete to understand heterogeneous reactivity.

The complex reaction pathways in the multigenerational oxidation of organic particles can be distilled into three fundamental transformation pathways: functionalization, fragmentation and oligomerization.[4,16−18] The overall rate at which these processes alter the chemical composition of a particle can be greatly enhanced via free radical chain propagation chemistry. Functionalization adds polar oxygenated functional groups to the organic particle without changing the particulate carbon content. This produces low volatility higher molecular weight oxygenated products, which results in an increase in the particle mass. Fragmentation produces lower molecular weight products via C−C bond scission along the carbon skeleton. These lower molecular weight oxidation products have higher vapor pressures and may evaporate from the particle, resulting in a detectable decrease in the particle mass (termed "volatilization"). Oligomerization produces higher molecular weight products via the covalent association of two organic species.

Recent studies on the OH-initiated oxidation of organic particles suggest that the heterogeneous oxidation rate and relative importance of functionalization and fragmentation reactions (i.e., reaction mechanism) depend upon the molecular structure of hydrocarbons in the particle. The heterogeneous oxidation rate is typically expressed as the heterogeneous reaction probability or the reactive uptake coefficient, defined as the fraction of gas−particle collisions that results in a reaction. Kessler et al.[19] found that while levoglucosan ($C_6H_{10}O_5$, a cyclic multifunctional oxygenated organic) particles reacted with OH radicals at a faster rate than erythritol ($C_4H_{10}O_4$, a straight chain alcohol), more particle volatilization is observed for the erythritol particles. Isaacman et al.[20] also reported that branched alkanes reacted at faster rates than straight chain alkanes in their study of the OH oxidation of motor oil particles. In addition, cyclic alkanes are observed to react with OH radicals at slower rates than normal and branched alkanes in their study of the OH oxidation of motor oil particles. This is in contrast to SAR estimates, which predict that cyclic alkanes would react faster due to the larger abundance of more reactive tertiary and secondary carbon atoms present in cyclic alkanes. These studies indicate that the dependence of heterogeneous reaction rates and mechanisms on the hydrocarbon's molecular structure remains poorly understood and should be an area of focus for further investigation.

In this work two model reaction systems, OH + squalene $C_{30}H_{50}$ and OH + unsaturated fatty acid (oleic acid $C_{18}H_{34}O_2$, linoleic acid $C_{18}H_{32}O_2$ and linolenic acid $C_{18}H_{30}O_2$), are analyzed to investigate the influence of molecular structure

(branched vs linear) and chemical functionality (alkene vs carboxylic acid) on the reaction rates and mechanisms in the OH-initiated oxidation of unsaturated organic particles. Squalene is a liquid branched alkene with 6 C=C double bonds, whereas oleic acid, linoleic acid and linolenic acid are liquid linear carboxylic acids with 1, 2, and 3 C=C double bonds, respectively (shown in Figure 1). The measurements for
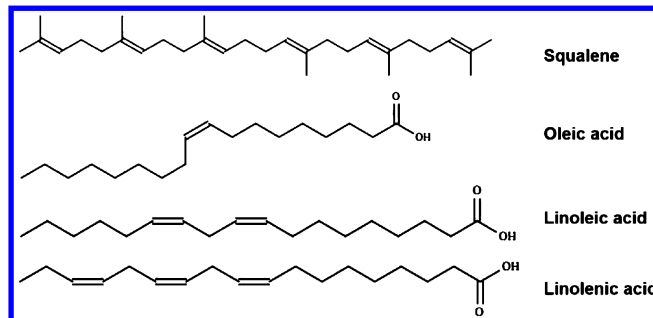

Figure 1. Chemical structures of squalene, oleic acid, linoleic acid, and linolenic acid.

the unsaturated fatty acid reactions have been previously reported,[21] while the measurements for the squalene reaction presented here are new. Since the oxidation kinetics and mechanisms of the three unsaturated fatty acids are similar,[21] for simplicity the kinetics and elemental analysis of the OH + squalene reaction are compared to measurements of the OH + linoleic acid reaction in this paper. We use the same experimental approach as the previous study of the OH + unsaturated fatty acid reactions[21] to examine the oxidation kinetics, products and mechanism of the OH + squalene reaction.

2. EXPERIMENT

The experimental setup employed in this study (shown in Figure 2) has been described in detail previously[21] and will be
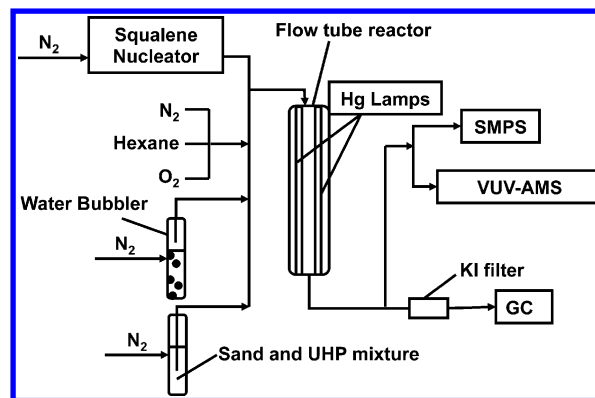
Figure 2. Experimental setup used to measure the OH-initiated oxidation of squalene aerosol.

discussed briefly here. Squalene aerosol particles are generated by homogeneous nucleation in a nitrogen (N_2) stream flowing through a Pyrex tube containing liquid squalene. The tube is heated in a furnace to ∼140 °C, producing a log−normal particle distribution with a mean surface weighted diameter of ∼224 nm and a geometric standard deviation of ∼1.4 nm. The particle flow is passed through an annular activated charcoal denuder to remove any residual gas-phase organics that may

have been formed in the furnace. A N_2/H_2O_2 gas mixture is introduced into the reactor by passing 0.05 to 0.15 L/min of N_2 through a heated bubbler (50 °C) that is packed with a 50:50 mixture of sand and urea hydrogen peroxide (UHP). Additional flows of humidified N_2, O_2 and tracer gas hexane (~150 ppb hexane in the flow reactor) are added to give a total flow rate of 1 L/min entering the flow reactor. The relative humidity in the flow reactor is fixed at 30%. $[O_2]$ in the flow reactor is reported here as a flow ratio. For experiments performed without O_2, a scrubber (0.75 L Supelpure-O trap) is placed in the N_2 lines to reduce the residual O_2 levels in the reactor to less than ~0.05%. An ozone monitor (2B Technologies Model 202), using an optical absorption cell at 254 nm, is used to measure $[H_2O_2]$ in the flow reactor prior to reaction. These measurements are corrected for the difference in the absorption cross sections of O_3 and H_2O_2 at 254 nm to quantify $[H_2O_2]$.

The particle/gas mixture is introduced into a quartz atmospheric pressure flow reactor that is 1.7 m long and has an inner diameter of 6.15 cm. OH radicals are formed in the reactor via the photolysis of H_2O_2 gas using four continuous output 130 cm long Hg lamps (λ = 254 nm) that are placed outside and along the length of the flow reactor. The reactor is cooled continuously using pressurized air. Based on the illuminated region of the reactor and the total flow rate going into the reactor (1 L/min), the reaction time is ~232 s. [OH] in the flow reactor ranges from 1×10^8 to 2×10^9 molec. cm^{-3}.

Particle size distributions exiting the flow reactor are measured by a scanning mobility particle sizer (SMPS, TSI Model 3936). The chemical composition of the aerosol is measured with a home-built vacuum ultraviolet photoionization (VUVPI) aerosol mass spectrometer (VUV-AMS) (mass resolution ~1500),[22] where the particles are thermally vaporized at 180 °C and photoionized by 9.6 eV VUV radiation produced by the Chemical Dynamics Beamline at the Advanced Light Source. For selected experiments, a high-resolution time-of-flight electron impact (EI) aerosol mass spectrometer (HR-ToF-AMS, Aerodyne Research Inc.) (mass resolution ~4300) is used to determine the average oxygen-to-carbon (O/C) and hydrogen-to-carbon (H/C) elemental molar ratios of the aerosol.[23−26] To correct for chemical biases that arise from ion fragmentation during the EI ionization process, the recommended correction factors of 0.75 for O/C and 0.91 for H/C are used for these measurements.[23,24]

A gas chromatograph (GC) equipped with a flame ionization detector (SRI model 8610C) is used to monitor the loss of the tracer gas hexane, which reacts with OH radicals at a rate constant (k_{Hex}) of 5.2×10^{-12} cm^3 molec^{-1} s^{-1}.[9] Particles and H_2O_2 are removed prior to the GC measurement using a particle filter and a potassium iodide (KI) trap, respectively. As described by previous publications from our group,[14,17−19,21,27] the OH exposure ([OH] × reaction time) is calculated from the decay of the hexane concentration during the reaction using relative rate analysis. The relative rate methodology relies on the assumption that the OH + hexane reaction dominates the loss of hexane in the flow reactor. Our group[27] previously verified that this is the case in our oxidation studies by using a kinetic model, which showed that OH accounts for 99% of the hexane lost during the reaction.

Since $[O_2]$ can influence the reaction rate, it is necessary to measure reaction rates at different $[O_2]$ in the reactor. In this set of experiments, at each $[O_2]$, the OH exposure is changed by varying the average OH concentration in the reactor by adjusting the photon flux of the Hg lamps (and hence the

photolysis rate of H_2O_2) while keeping the total flow rate (i.e., reaction time) constant. Since the absolute [OH] in the reactor can also influence reaction rates, experiments are conducted at different absolute [OH] in the reactor. In this set of experiments, at each absolute [OH], the OH exposure is changed by adjusting the reaction time. As described by previous publications from our group,[14,21] this is achieved by fixing the total flow rate while moving an opaque curtain along the length of the flow reactor. This changes the residence time of the aerosol in the illuminated region of the reactor and hence the reaction time.

The reaction between OH radicals and squalene particles is second-order. The decay in the relative intensities of the squalene ion peaks in the VUVPI mass spectrum is measured as a function of OH exposure. The rate constant (k_{Sqe}, cm^3 molec^{-1} s^{-1}) is computed using the standard relative rate methodology described by Hearn et al.[28] and Smith et al.[27] The normalized decay of particle-phase squalene is compared with the normalized decay of hexane,

$$\ln([Sqe]/[Sqe]_0) = k_{Sqe}\left(\frac{\ln([Hex]/[Hex]_0)}{k_{Hex}}\right) \quad (1)$$

where $[Sqe]$ and $[Sqe]_0$ are the final and initial concentrations of particle-phase squalene, $[Hex]$ and $[Hex]_0$ are the final and initial concentrations of hexane, and k_{Hex} is the rate constant for the reaction of hexane with OH radicals. Smith et al.[27] showed that the bracketed portion on the right-hand side of eq 1 is equal to the average OH exposure ($\langle OH \rangle_t \cdot t$) and can be expressed as

$$\frac{\ln([Hex]/[Hex]_0)}{-k_{Hex}} = \int_0^t [OH]\, dt = \langle OH \rangle_t \cdot t \quad (2)$$

where [OH] is the time dependent OH concentration. Equation 2 can be substituted into eq 1 and converted into exponential form to obtain the normalized decay of particle-phase squalene,

$$\frac{[Sqe]}{[Sqe]_0} = \exp(-k_{Sqe} \cdot \langle OH \rangle_t \cdot t) \quad (3)$$

Assuming that k_{Sqe} is independent of [OH], $[Sqe]/[Sqe]_0$ can be plotted against $\langle OH \rangle_t \cdot t$ and fit to an exponential function to obtain k_{Sqe}. The effective uptake coefficient for squalene (γ_{eff}^{Sqe}), defined as the number of particle-phase squalene molecules reacted per OH-particle collision, can be expressed as[27]

$$\gamma_{eff}^{Sqe} = \frac{2 \cdot k_{Sqe} \cdot D_{surf} \cdot \rho_0 \cdot N_A}{3 \cdot \overline{c} \cdot M_{Sqe}} \quad (4)$$

where D_{surf} is the mean surface-weighted particle diameter, ρ_0 is the initial squalene density, N_A is Avogadro's number, $\overline{c}$ is the mean speed of gas-phase OH, and M_{Sqe} is the molar mass of squalene. γ_{eff}^{Sqe} includes contributions from both the heterogeneous reaction of OH radicals with squalene and secondary chain reactions, and therefore, it can be larger than one. This differs from the aforementioned reactive uptake coefficient (in the Introduction), which only considers the fraction of OH−particle collisions that results in a reaction of squalene, thus necessitating it to be less than or equal to unity.

Equation 4 assumes that the squalene decay rate is directly proportional to the concentration of particle-phase squalene, which is the case when the particle is internally well-mixed on the time scale of the reaction (i.e. mixing in the particle is

sufficiently fast such that unreacted squalene molecules are continuously replenished at the particle surface).[27] The assumption that the reaction is not limited by the diffusion of squalene molecules to the particle surface is reasonable since the estimated time scale for the reactive loss of squalene ($1/(k_{Sqe}\cdot[OH])$, s) is several orders of magnitude ($\sim 4 \times 10^6$) longer than the mixing time in the particle.[29] The validity of these assumptions will be discussed further in section A.

3. RESULTS: OH + SQUALENE

In section A, the oxidation products and kinetics of the OH + squalene reaction are presented. Measurements showing how $[O_2]$ and $[OH]$ in the reactor influence the values of γ_{eff}^{Sqe} are presented in section B. Elemental analysis of squalene particles is presented in section C. These kinetic and elemental composition measurements are compared to previously reported measurements of the OH + linoleic acid reaction.[21]

A. Oxidation Products and Kinetics. VUVPI mass spectrometry is used to identify products and determine γ_{eff}^{Sqe}. The mass spectra of squalene particles before and after reaction are shown in parts a and b, respectively, of Figure 3. For more
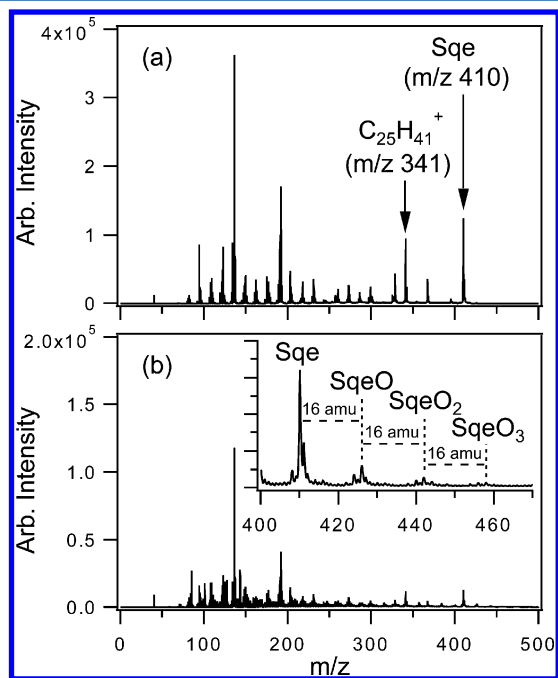
Figure 3. VUVPI mass spectrum of squalene (Sqe) particles, measured at a photoionization energy of 9.6 eV: (a) before and (b) after exposure to OH radicals ($\sim 2.6 \times 10^{11}$ molecules cm^{-3} s) at $[H_2O_2] = 18.5$ ppm and $[O_2] = 10\%$. The two squalene VUV ion peaks (m/z 410 and 341) monitored during the kinetic measurements are shown in panel (a). The inset in panel (b) shows the higher molecular weight oxygenated reaction products (labeled as SqeO, SqeO$_2$, and SqeO$_3$ to denote the number of oxygen atoms added to the squalene molecule) formed during the reaction.

precise kinetic measurements, both the squalene molecular ion (m/z 410) and the C$_{25}$H$_{41}^{+}$ fragment ion (m/z 341) are monitored during the reaction. Upon exposure to OH radicals, the intensities of the squalene molecular ion and the C$_{25}$H$_{41}^{+}$ fragment ion decrease, and groups of higher molecular weight products centered at m/z 426, 442, and 458 (shown in Figure 3b inset) are formed.

Based on the masses of the higher molecular weight reaction products, these products appear to contain oxygenated functional groups in the form of carbonyls and alcohols. As fragmentation patterns and photoionization efficiencies may depend on the identity of the parent molecule, it is difficult to obtain absolute product yields of specific species (e.g., alcohols vs ketones) within the same group of peaks based on the relative peak intensities in the mass spectrum. As such, detailed isomer product analyses will be presented in a forthcoming publication. Here for simplicity, the first three groups of higher molecular weight products are referred to as SqeO, SqeO$_2$, and SqeO$_3$ to denote the number of oxygenated functional groups (i.e., alcohols and ketones) added to the squalene molecule.

A similar set of higher molecular weight reaction products was observed for the OH + unsaturated fatty acid reactions,[21] which serve as a useful starting point for understanding product formation chemistry in the OH + squalene reaction. Figure 4 shows a plausible general reaction scheme for the OH-initiated oxidation of unsaturated organic particles. This reaction scheme only applies to products formed by OH addition to the C=C double bond. Once all the C=C double bonds in the particle have reacted (and are replaced by C−C bonds), further particle oxidation is expected to take place via H atom abstraction by OH radicals.[15−19,27,28,30−32] In Figure 4, the substituent X on the carbon in the C=C double bond refers to CH$_3$ for squalene (and H for the unsaturated fatty acids).

Previous gas-phase[7,8,10,33,34] and monolayer[35,36] studies of the reaction of OH radicals with unsaturated organics suggest that the OH + squalene reaction is initiated predominantly via OH addition to the C=C double bond to form a hydroxyalkyl radical. While the OH radical can add to either carbon in the C=C double bond, SARs[12] predict that OH addition to the less substituted carbon (to form tertiary hydroxyalkyl radicals) occurs ~ 2 times faster than OH addition to the more substituted carbon of the C=C double bond (to form secondary hydroxyalkyl radicals). This is due to the enhanced stability of tertiary hydroxyalkyl radicals relative to secondary hydroxyalkyl radicals.

In the absence of O$_2$, the hydroxyalkyl radical can react heterogeneously with a gas-phase OH radical to form a diol (R3 in Figure 4), or abstract a H atom from a neighboring squalene molecule (or its products) in the particle to form an alkyl (R$^{\bullet}$) radical and an alcohol (R2 in Figure 4). When O$_2$ is present, the hydroxyalkyl and R$^{\bullet}$ radicals can react with O$_2$ to form hydroxyperoxy (R4 in Figure 4) and peroxy (not shown) radicals, respectively. The hydroxyperoxy radical can then react with another hydroxyperoxy radical or a peroxy radical to form either stable oxygenated products (e.g., alcohols and ketones) via the Bennett−Summers and Russell mechanisms (R5 in Figure 4), or hydroxyalkoxy radicals (R6 in Figure 4).[37−40] The hydroxyalkoxy radicals can then dissociate via C−C bond scission to form lower molecular weight products (R7 in Figure 4), or abstract a H atom from a neighboring squalene molecule (or its products) to form a diol and a R$^{\bullet}$ radical (R8 in Figure 4). Ketone formation via the hydroxyalkoxy radical + O$_2$ reaction is not shown in Figure 4 since tertiary hydroxyalkoxy radicals (which are expected to be formed in high yields in the presence of O$_2$) do not have H atoms adjacent to the peroxy radical available for abstraction by O$_2$. The isomerization of the hydroxyalkoxy radical is also not shown in Figure 4 since there is no strong evidence for this pathway from the experimental data.
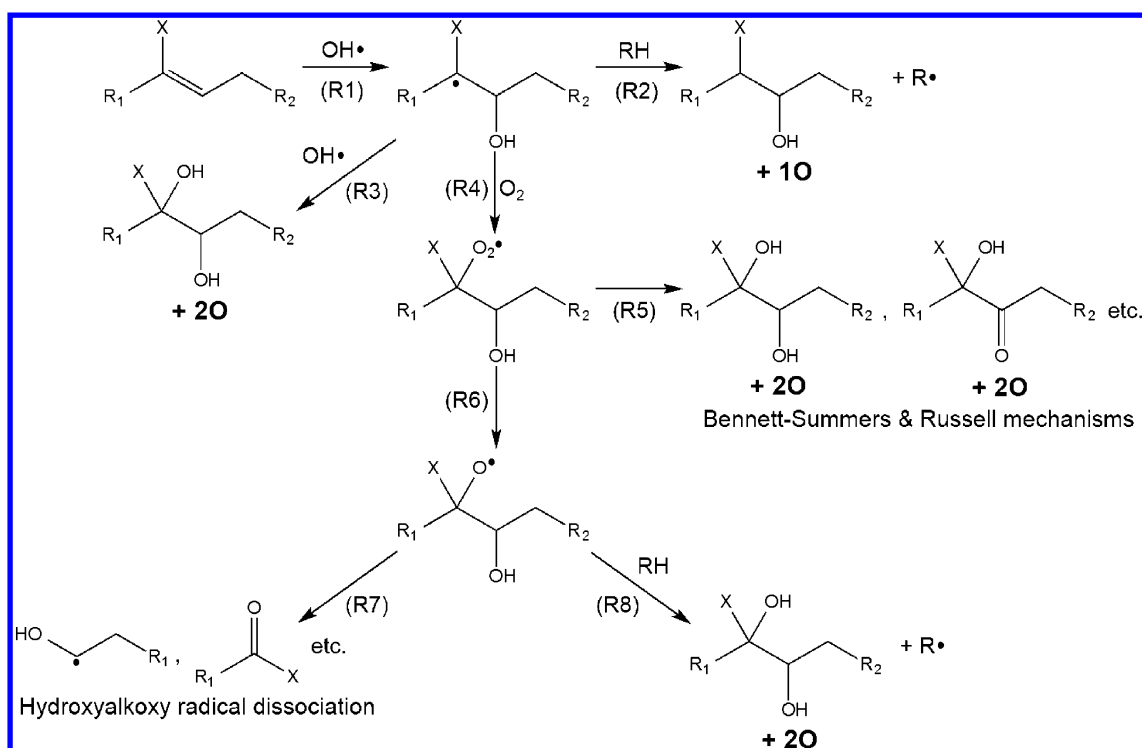
Figure 4. Proposed general reaction scheme for the OH-initiated oxidation of unsaturated organic (RH) particles. The substituent X on the carbon in the C=C double bond refers to CH_3 for squalene and H for the unsaturated fatty acids. R• represents the generic alkyl radical formed by the abstraction of a hydrogen atom from the unsaturated organic molecule. The number of O atoms added to the unsaturated organic molecule for the various reaction pathways are also shown.

The SqeO products in Figure 3b can be explained by the formation of alcohols (with masses 426 and 428 amu) from the reaction of OH radicals with R• radicals (not shown in Figure 4) and H atom abstraction reaction by hydroxyalkyl radicals (R2 in Figure 4), respectively. Previous studies have also shown that, in the presence of O_2, peroxy radicals undergo self-reaction to form first generation products with one carbonyl group (with mass 424 amu) or one alcohol group (with mass 426 amu).[27,30−32,37−40] These reaction pathways suggest that SqeO is made up of first generation products (i.e., products formed via a single reaction with OH).

While SqeO is made up solely of first generation products, $SqeO_2$ can in principle contain both first and second generation products. First generation $SqeO_2$ products can be formed from the reaction of hydroxyalkyl radicals with OH radicals (R3 in Figure 4), from a hydroxyperoxy radical + hydroxyperoxy/peroxy radical reaction (R5 in Figure 4), or via H atom abstraction by hydroxyalkoxy radicals (R8 in Figure 4). Second generation $SqeO_2$ products can be formed from the reaction of first generation SqeO with OH radicals. Analogously, $SqeO_3$ contains both second and third generation products.

To measure the kinetics of the squalene reaction, the decays in the relative intensities of the squalene molecular ion and the $C_{25}H_{41}^+$ fragment ion in the mass spectra are measured as a function of OH exposure. For this measurement, the OH exposure is changed by adjusting the photon flux of the Hg lamps while keeping the reaction time and $[H_2O_2]$ fixed. Parts a and b of Figure 5 show the normalized decay curves for squalene ($[Sqe]/[Sqe]_0$) as a function of OH exposure in the presence of 18.5 ppm $[H_2O_2]$ at ∼0% and 10% $[O_2]$, respectively. The decay of squalene is well-represented by an exponential function, thus confirming our original assumption

that the squalene decay rate is directly proportional to the concentration of particle-phase squalene and the reaction is not limited by the diffusion of squalene molecules to the particle surface.

The squalene decays shown in Figure 5a and b are fit to eq 3 to obtain k_{Sqe}, which is used to compute γ_{eff}^{Sqe} using eq 4. The γ_{eff}^{Sqe} values measured at 18.5 ppm $[H_2O_2]$ are 1.47 ± 0.06 and 2.34 ± 0.07 at ∼0% and 10% $[O_2]$, respectively. This indicates that more than one particle-phase squalene molecule is lost for every OH−particle collision and is clear evidence for secondary chain chemistry. Due to unknown amounts of secondary chemistry, γ_{eff}^{Sqe} is not corrected for gas-phase diffusion. The relationship between γ_{eff}^{Sqe} and $[O_2]$ will be discussed further in section C.

Waring et al.[41] previously studied the reaction of hyperthermal OH radicals on a liquid squalene surface at low pressure. By measuring the reactive loss of gas-phase OH radicals (as opposed to the loss of condensed-phase squalene molecules in this study), they determined that the reactive uptake coefficient (γ_{OH}) is 0.39 ± 0.07. Assuming that γ_{OH} for the surface reaction of OH radicals with squalene particles is 0.39, dividing γ_{eff}^{Sqe} by γ_{OH} allows us to place an upper limit on the chain propagation length in our study. The chain propagation length is the number of squalene molecules that are removed for every reactive OH−particle collision. At ∼ 0% $[O_2]$, the chain propagation length is 3.77. This suggests that, for every particle-phase squalene molecule consumed by a heterogeneous reaction with a OH radical, ∼3 other squalene molecules are consumed by secondary reactions. At 10% $[O_2]$, the chain propagation length increases to 6.

The evolution of squalene and its higher molecular weight products are measured as a function of OH exposure to
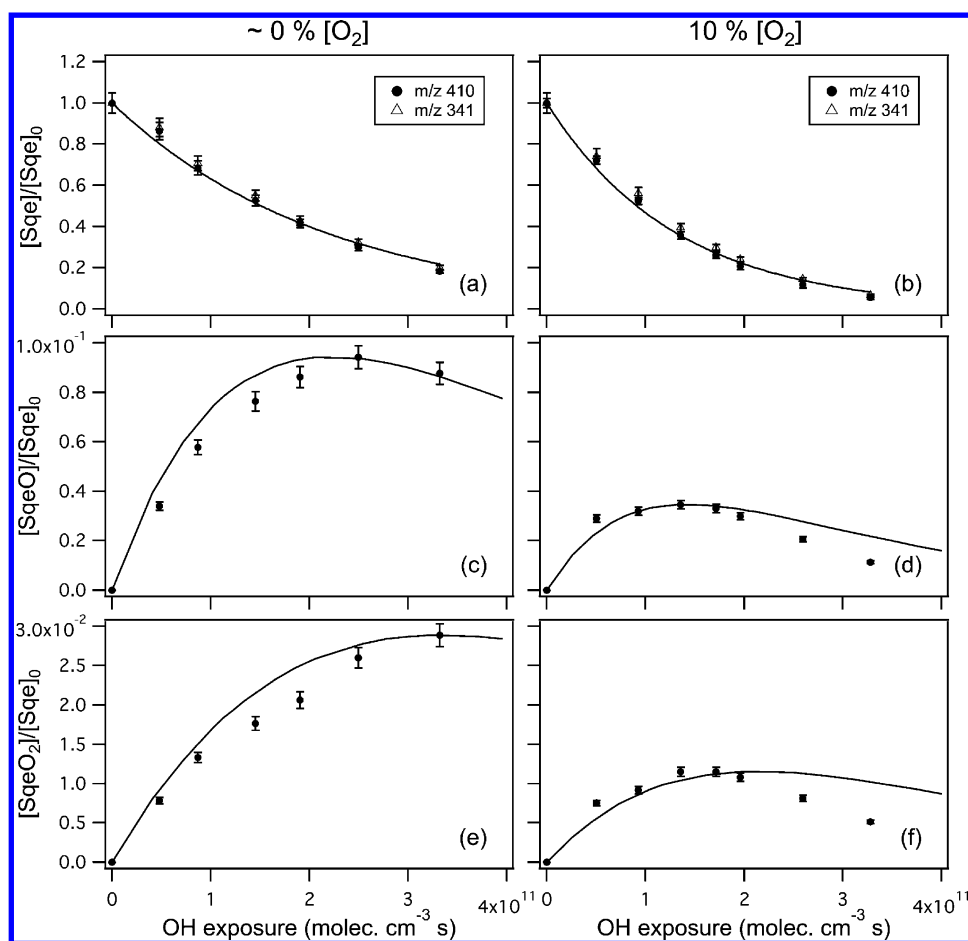
Figure 5. Evolution of squalene, SqeO, and $SqeO_2$ as a function of OH exposure at $[H_2O_2]$ = 18.5 ppm for (a, c, and e) $[O_2]$ = ∼ 0% and (b, d, and f) $[O_2]$ = 10%. In panels (a) and (b), the decays of squalene are fit using eq 3 to obtain k_{Sqe} (solid line). The solid lines in panels (c) to (f) are model predictions calculated using SAR predictions,[11] which serve as a comparison to the measured product evolutions. The uncertainties represent the standard deviations of individual measurements made at each OH exposure.

understand how the reactivity of squalene differs from that of its products. Parts a, c, and e of Figure 5 show the evolution of squalene, SqeO, and $SqeO_2$ versus OH exposure at ∼0% $[O_2]$, respectively. The evolution of SqeO and $SqeO_2$ are compared to SAR calculations to identify similarities and differences between heterogeneous and homogeneous gas-phase oxidation reactions. For simplicity, the first and second generation higher molecular weight products of squalene are assumed to have 5 and 4 C═C double bonds, respectively, in the SAR calculations. The predicted reaction rates of these higher molecular weight products (relative to that of squalene) are calculated based solely on the number and type of reaction sites (e.g., number of C═C bonds) present in these products. For simplicity, we also assume that the reaction rates of all the secondary chain reactions scale proportionately with the number and type of reaction sites present in these products in the SAR calculations. SAR[11] calculations predict that the first and second generation higher molecular weight products would react at rates ∼15 and 30% slower than those of squalene, respectively, since these products have fewer C═C double bonds for reaction (relative to squalene). A kinetic model predicting the evolution of SqeO and $SqeO_2$ is constructed based on SAR predictions (shown as solid lines in Figure 5c and e). Parts c and e of Figure 5 show that SqeO and $SqeO_2$ reach their maxima at OH exposures slightly larger than those predicted by SAR calculations, indicating that the formation

and reaction of SqeO and $SqeO_2$ occur at rates slightly slower than that predicted by SAR calculations.

Similar calculations are performed on the evolution of squalene, SqeO, and $SqeO_2$ at 10% $[O_2]$ in parts b, d, and f, respectively, of Figure 5. The kinetic behavior of SqeO and $SqeO_2$ are again compared with SAR[11] calculations (shown as solid lines in Figure 5d and f). Parts d and f of Figure 5 show that SqeO and $SqeO_2$ peak at OH exposures smaller than those predicted by SAR calculations. This indicates that SqeO and $SqeO_2$ are formed and react at rates faster than that predicted by SAR calculations.

It is unclear why the formation and reaction rates of SqeO and $SqeO_2$ are faster than that predicted by SAR calculations at 10% $[O_2]$ but are slightly slower than the rates predicted by SAR calculations at ∼0% $[O_2]$. However, analogous to the OH + linoleic acid reaction,[21] the deviation in the evolution of SqeO and $SqeO_2$ from SAR predictions at ∼0 and 10% $[O_2]$ can be attributed to differences between the gas−particle interface and a homogeneous gas-phase environment. SAR calculations also do not consider secondary chain reactions that may accelerate the reactive depletion rate of squalene. The high molecular density in the squalene particle may enhance these particle-phase chain cycling reactions, and consequently, these reactions accelerate the overall rate of particle transformation.

Based on the reaction scheme shown in Figure 4, the particle-phase secondary chain reactions that accelerate the

reactive depletion rate of squalene are H atom abstraction reactions by hydroxyalkyl and hydroxyalkoxy radicals (R2 and R8 in Figure 4, respectively). Squalene has 44 H atoms from C(sp³)−H bonds available for abstraction, while the abstraction of H atoms attached to C=C double bonds is energetically unfavored.[42,43] The 44 H atoms from the C(sp³)−H bonds in squalene are allylic in nature, since they are attached to C atoms that are adjacent to C=C double bonds. Previous studies have shown that allylic C−H bonds have significantly lower bond energies than their equivalents in saturated hydrocarbons.[42,43] In the OH + squalene reaction, the lower allylic C−H bond energies may potentially result in larger rate constants for the H atom abstraction reactions by hydroxyalkyl and hydroxyalkoxy radicals.

Since the allylic C−H bonds of squalene are weaker than their equivalents in saturated hydrocarbons, H atom abstraction by OH radicals may play a role in the OH + squalene reaction. It is difficult to ascertain the relative contributions of OH addition and H atom abstraction to γ_{eff}^{Sqe} from the experimental data. However, in a study of the OH oxidation of 3-methyl-1-butene, Atkinson et al.[33] showed that H atom abstraction by OH radicals from the allylic C−H bond in 3-methyl-1-butene is a minor reaction channel (relative to OH addition to the C=C double bond) at room temperature. A study of the OH oxidation of 1-butene also reported that products derived from H atom abstraction reactions by OH radicals are not observed despite the presence of an allylic C−H bond.[34]

In the OH + squalene reaction, the allylic R• radicals formed from H atom abstraction reactions are resonance stabilized and have 6 C=C double bonds. The structures of these resonance-stabilized allylic R• radicals may influence the type of stable products formed from the reaction of allylic R• radicals with O₂ and OH radicals. For example, despite the abstraction of a secondary H atom from an allylic C−H bond, a tertiary allylic R• radical may be formed as a result of resonance stabilization. The tertiary allylic R• radicals can react with O₂ to form tertiary peroxy radicals. Kroll et al.[17] showed that the formation of higher molecular weight oxygenated products via the Bennett−Summers and Russell mechanisms[37−40] is suppressed in the reaction between two tertiary peroxy radicals (due to the lack of H atoms adjacent to the peroxy radical), and tertiary alkoxy radicals are likely the dominant products. These tertiary alkoxy radicals can then dissociate to form lower molecular weight oxygenated products. A detailed analysis on the products derived from the formation of these allylic R• radicals will be presented in a forthcoming paper.

B. Effective Uptake Coefficient vs [O₂] and [OH]. Figure 6a shows how γ_{eff}^{Sqe} changes as a function of [O₂] in the flow reactor at 1.4 ± 0.2 and 18.5 ± 0.4 ppm [H₂O₂]. For both H₂O₂ concentrations, γ_{eff}^{Sqe} increases before leveling off when [O₂] is increased. γ_{eff}^{Sqe} is 1.55 ± 0.05 and 1.47 ± 0.06 at ∼0% [O₂], and increases to 2.59 ± 0.12 and 2.27 ± 0.08 at 18% [O₂] for 1.4 and 18.5 ppm [H₂O₂], respectively.

The increase in γ_{eff}^{Sqe} with increasing [O₂] is much different from the trend observed in the OH + linoleic acid reaction,[21] where the effective uptake coefficient for the linoleic acid (γ_{eff}^{LA}) decreases with increasing [O₂] instead. Generally, the inverse relationship between γ_{eff}^{LA} and [O₂] is attributed to the role that O₂ predominantly plays in promoting chain termination reactions.[14,21] In the absence of O₂, the hydroxyalkyl radical formed from the initial OH addition to the C=C double bond in the linoleic acid propagates the particle-phase secondary chain chemistry by reacting with other linoleic acid molecules.
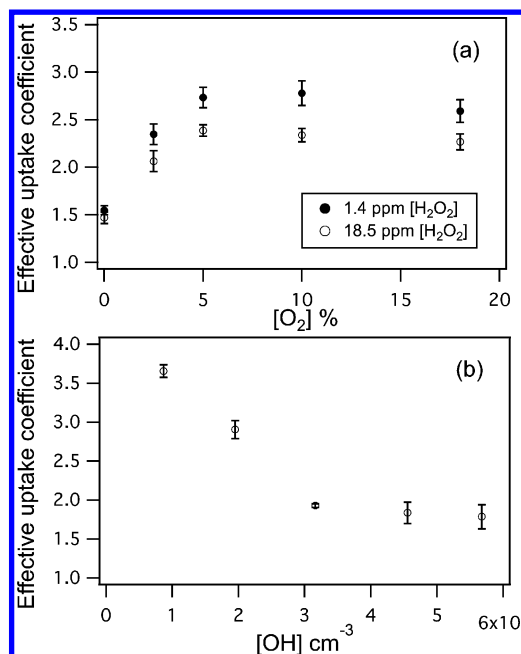

Figure 6. (a) Effective uptake coefficients of squalene as a function of [O₂] at 1.4 ppm [H₂O₂] and 18.5 ppm [H₂O₂]. (b) Effective uptake coefficients of squalene as a function of [OH] at [H₂O₂] = 18.5 ppm and [O₂] = 10%. The uncertainties represent the standard deviations of individual measurements.

When increasing amounts of O₂ are added to the reaction, the chain reaction slows since the hydroxyalkyl radicals can react instead with O₂ to form hydroxyperoxy radicals that can undergo self-reactions to form terminal oxygenated products (i.e., chain termination). This causes γ_{eff}^{LA} to decrease with increasing [O₂]. Here the increase in γ_{eff}^{Sqe} with increasing [O₂] implies that O₂ predominantly promotes chain propagation reactions. This suggests that the chain cycling mechanism in the OH + squalene reaction may be different from the OH + linoleic acid reaction. These differences will be further discussed in section 4.

Figure 6a also shows that γ_{eff}^{Sqe} values measured at 1.4 ppm [H₂O₂] are larger than those measured at 18.5 ppm [H₂O₂]. This is consistent with the trend observed in the OH + linoleic acid reaction,[21] where the inverse relationship between γ_{eff}^{LA} and the concentration of the radical precursor (H₂O₂) is explained by H₂O₂ impeding the OH reaction of linoleic acid particles by adsorbing to the particle surface and blocking reaction sites. A similar inverse relationship between the concentration of the radical precursor (O₃) and the effective uptake coefficient is also observed by Renbaum et al.[44] in their study of the OH oxidation of 2-octyldodecanoic acid aerosol. In that study, the effective uptake coefficients are interpreted using a Langmuir-type isotherm, which suggests that O₃ adsorbs to the surface of the 2-octyldodecanoic acid particles and blocks reaction sites at the particle surface. Analogous to the OH + 2-octyldodecanoic acid[44] and OH + linoleic acid[21] reactions, it is possible that H₂O₂ impedes the OH reaction of squalene particles by adsorbing to the particle surface and blocking reaction sites. This is one explanation for why γ_{eff}^{Sqe} values measured at 1.4 ppm [H₂O₂] are larger than those measured at 18.5 ppm [H₂O₂].

Since H₂O₂ is the radical precursor, the relationship between γ_{eff}^{Sqe} and [H₂O₂] may also be coupled to the relationship of γ_{eff}^{Sqe} with the absolute [OH]. Figure 6b shows γ_{eff}^{Sqe} as a function of [OH] at 18.5 ppm [H₂O₂] for 10% [O₂]. For this set of
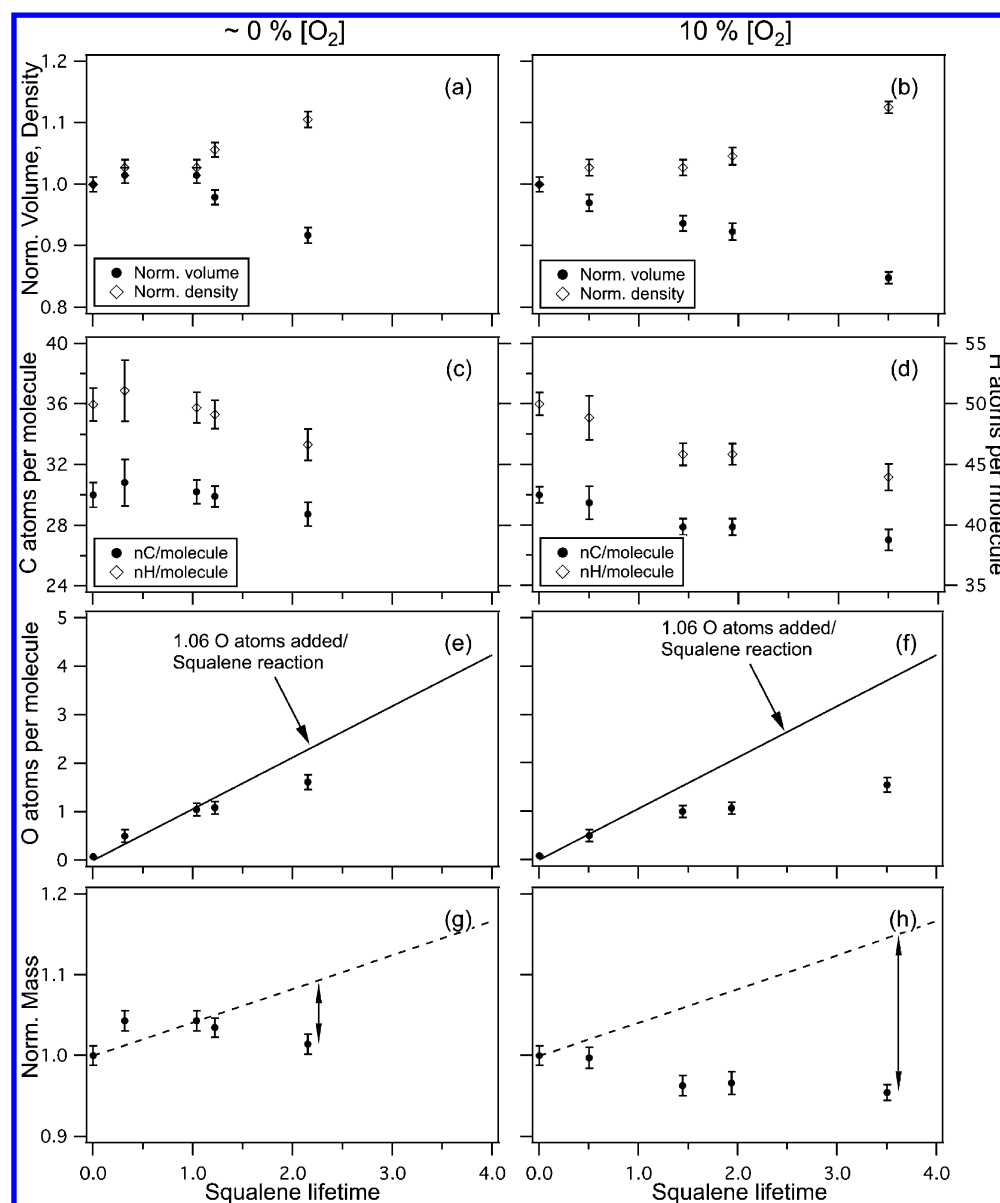
Figure 7. Elemental analysis of squalene particles as a function of squalene lifetime at $[H_2O_2]$ = 20.7 ppm for (a, c, e, and g) $[O_2]$ = ∼ 0% and (b, d, f, and h) $[O_2]$ = 10%. Panels (a) and (b): particle volume and density (normalized to the initial volume and density per unreacted particle). Panels (c) and (d): average number of C and H atoms per squalene molecule. Panels (e) and (f): average number of O atoms per squalene molecule. Panels (g) and (h): aerosol mass (normalized to the initial mass per unreacted particle). In panels (e) and (f), the initial increase in the average number of O atoms per squalene molecule is fit using the linear function mx (solid lines). In panels (g) and (h), the measured particle mass data is compared with the particle mass predictions (dashed lines) based on the assumption that 1.06 O atoms are added per reactive loss of squalene. The degree of particle volatilization is the difference between the measured particle mass and the predicted mass (arrows).

measurements, the OH exposure is changed by varying the reaction time while fixing $[H_2O_2]$ and $[OH]$. γ_{eff}^{Sqe} decreases when the absolute $[OH]$ in the flow reactor increases.

The inverse relationship between γ_{eff}^{Sqe} and $[OH]$ is similar to observations made in the OH + linoleic acid reaction[21] where the inverse relationship is attributed to the presence of chain termination reactions involving OH radicals. These chain termination reactions compete with chain propagation reactions by consuming OH radicals that would otherwise react with linoleic acid molecules. This slows the chain reaction down, causing γ_{eff}^{LA} to decrease with increasing absolute $[OH]$. A study by Liu et al.[14] on the Cl + squalane reaction similarly attributed the inverse relationship between the effective uptake coefficient and $[Cl]$ to chain termination reactions involving Cl

atoms. Analogous to the OH + linoleic acid[21] and Cl + squalane[14] reactions, OH radicals can react with hydroxyalkyl, $R^\bullet$, and other OH radicals to form terminal products (i.e., diols, alcohols, and H_2O_2, respectively) in the OH + squalene reaction. These chain termination reactions consume OH radicals and slow the radical chain chemistry in the particle, and thus could explain the inverse relationship between γ_{eff}^{Sqe} and $[OH]$.

C. Elemental Analysis. The relative importance of functionalization and fragmentation pathways can be determined from how the average aerosol mass and elemental content evolve during the reaction. EI-MS is used to measure the elemental O/C and H/C ratios and aerosol mass. The particle mass is obtained from the product of the particle

volume (measured by the SMPS) and the particle density, which is computed from the ratio of the vacuum aerodynamic diameter (measured by the HR-ToF-AMS) and the mobility diameter (measured by the SMPS).[17,45] As shown by Kroll et al.,[17] the average particulate carbon content (the average number of C atoms in the particle phase, nC) can be expressed as

$$nC = \frac{M}{12 + 16(O/C) + (H/C)} \qquad (5)$$

where M is the particle mass and O/C and H/C are the elemental ratios. The average number of C atoms present in the squalene molecule is obtained from the product of the average particulate carbon content (normalized to the initial amount of particulate carbon) and the initial number of C atoms in the squalene molecule ($N_C = 30$). The average number of O and H atoms present in the squalene molecule is obtained by multiplying the O/C and H/C ratios with the average number of C atoms present in the squalene molecule.

Figure 7 shows the mass measurements and elemental analysis of squalene particles as a function of squalene lifetime at 20.7 ppm [H$_2$O$_2$] for ~0 and 10% [O$_2$]. The squalene lifetime (τ_{Sqe}) is

$$\tau_{Sqe} = k_{Sqe} \cdot \langle OH \rangle_t \cdot t \qquad (6)$$

where k_{Sqe} is the measured rate constant for squalene and $\langle OH \rangle_t \cdot t$ is the measured OH exposure.[27] The squalene lifetime represents the number of reactive events (i.e., heterogeneous and/or homogeneous reactions that consume the molecular species) that an average particle-phase squalene molecule has undergone.[17,18,27] At one lifetime, the number of reactive events equals the number of molecules in the particle. These measurements are plotted as a function of squalene lifetime to show the changes in particle mass and elemental composition per squalene reaction.

Parts a and b of Figure 7 show that particle density increases with oxidation at both ~0 and 10% [O$_2$]. This increase in density as the particles become increasingly oxidized is consistent with previous density measurements of oxidized organic aerosol.[17,31] Figure 7a also shows that, at ~0% [O$_2$], particle volume increases slightly when oxidation is first initiated before decreasing after ~1 squalene lifetime. In contrast, Figure 7b shows that particle volume decreases monotonically at 10% [O$_2$].

Figure 7c shows that, at ~0% [O$_2$], the average number of C atoms in the squalene molecule stays roughly constant at 30 (within experimental error) when oxidation is first initiated (0 to ~1 squalene lifetimes) before decreasing to 28.7 ± 0.8 upon further oxidation. The average number of H atoms in the squalene molecule first increases to 51.1 ± 2.5 before decreasing to 46.7 ± 1.3 upon further oxidation. In contrast, measurements recorded at 10% [O$_2$] (shown in Figure 7d) show that the average numbers of C and H atoms in the squalene molecule decrease immediately to 27.0 ± 0.7 and 44.0 ± 1.1, respectively, once oxidation occurs.

Parts e and f of Figure 7 show that, at both ~0 and 10% [O$_2$], the average number of O atoms in the squalene molecule increases linearly during the early stages of oxidation, before slowing upon further oxidation. One possible explanation for this change in the net rate of O atom addition is the increased importance of fragmentation reactions as oxidation progresses.[17,18,27] Fragmentation leads to the formation of lower

molecular weight products, which have higher vapor pressures and may evaporate from the particle. As a result, a significant fraction of particulate O (and C and H) atoms leaves the particle as gas-phase products, causing the net rate of O atom addition to the particle to slow.

To estimate the average number of O atoms added to the particle per reactive loss of squalene during the initial stages of oxidation, the initial increase in the average number of O atoms per squalene molecule at ~0% [O$_2$] is fit with a line (shown as a solid line in Figure 7e). Particle volatilization (i.e., fragmentation) is negligible over this range since Figure 7c shows that the average number of C atoms in the squalene molecule stays roughly constant at 30, thus indicating little particulate carbon loss (and hence little particle volatilization). From 0 to ~1 squalene lifetimes, the average number of O atoms added per squalene reacted increases linearly with a slope of 1.06 ± 0.12. This suggests that an average of 1.06 ± 0.12 O atoms are added per reactive loss of squalene prior to the onset of particle volatilization. Similarly, Figure 7f shows that ~1.06 O atoms are added per reactive loss of squalene from 0 to ~0.5 squalene lifetimes (shown as a solid line in Figure 7f) at 10% [O$_2$]. At squalene lifetimes >0.5, the increase in particulate oxygen content starts to slow due to particle volatilization.

One might expect an average of two O atoms added per squalene reacted (from the formation of diols and hydroxycarbonyls) if the Bennett−Summers and Russell mechanisms[37−40] (R5 in Figure 4) are dominant pathways in the OH + squalene reaction. Instead the addition of 1.06 O atoms per reactive loss of squalene (at early lifetimes) indicates that secondary chain reactions play significant roles in the OH + squalene reaction.

To better understand how O$_2$ influences particle volatilization, particle mass measurements are compared with mass predictions (shown as dashed lines in Figure 7g and h) based on measurements that an average of 1.06 O atoms are added per reactive loss of squalene at ~0 and 10% [O$_2$]. H atom addition/loss is not considered in the mass predictions due to the relatively minor mass contribution of H atoms (~2%) to the overall change in the particle mass.

Figure 7g shows that the average particle mass increases at early squalene lifetimes (0 to ~1 squalene lifetimes) for ~0% [O$_2$], which is consistent in magnitude with an increase in particulate oxygen content as described above. The measured particle mass and predicted particle mass are similar from 0 to ~1 squalene lifetimes, indicating that functionalization reactions (which add oxygenated functional groups to the particle) are important during the initial stages of oxidation, with fragmentation reactions being a minor pathway. The measured particle mass starts to decrease after ~1 squalene lifetimes and deviates increasingly from the predicted mass upon further reaction. This signals the increasing importance of fragmentation reactions, which may form volatile products that evaporate from the particle. Figure 7h shows that, at 10% [O$_2$], the average particle mass decreases immediately upon oxidation and deviates increasingly from the predicted mass with increasing squalene lifetime. This indicates that particle volatilization occurs even at the early stages of oxidation, and it suggests that fragmentation is an important reaction channel when O$_2$ is present in the reaction. This difference in the evolution of squalene particle mass (0% vs 10% [O$_2$]) implies that O$_2$ promotes fragmentation reactions in the OH + squalene reaction. In addition, previous studies showed that

4114

dx.doi.org/10.1021/jp502666g | J. Phys. Chem. A 2014, 118, 4106−4119
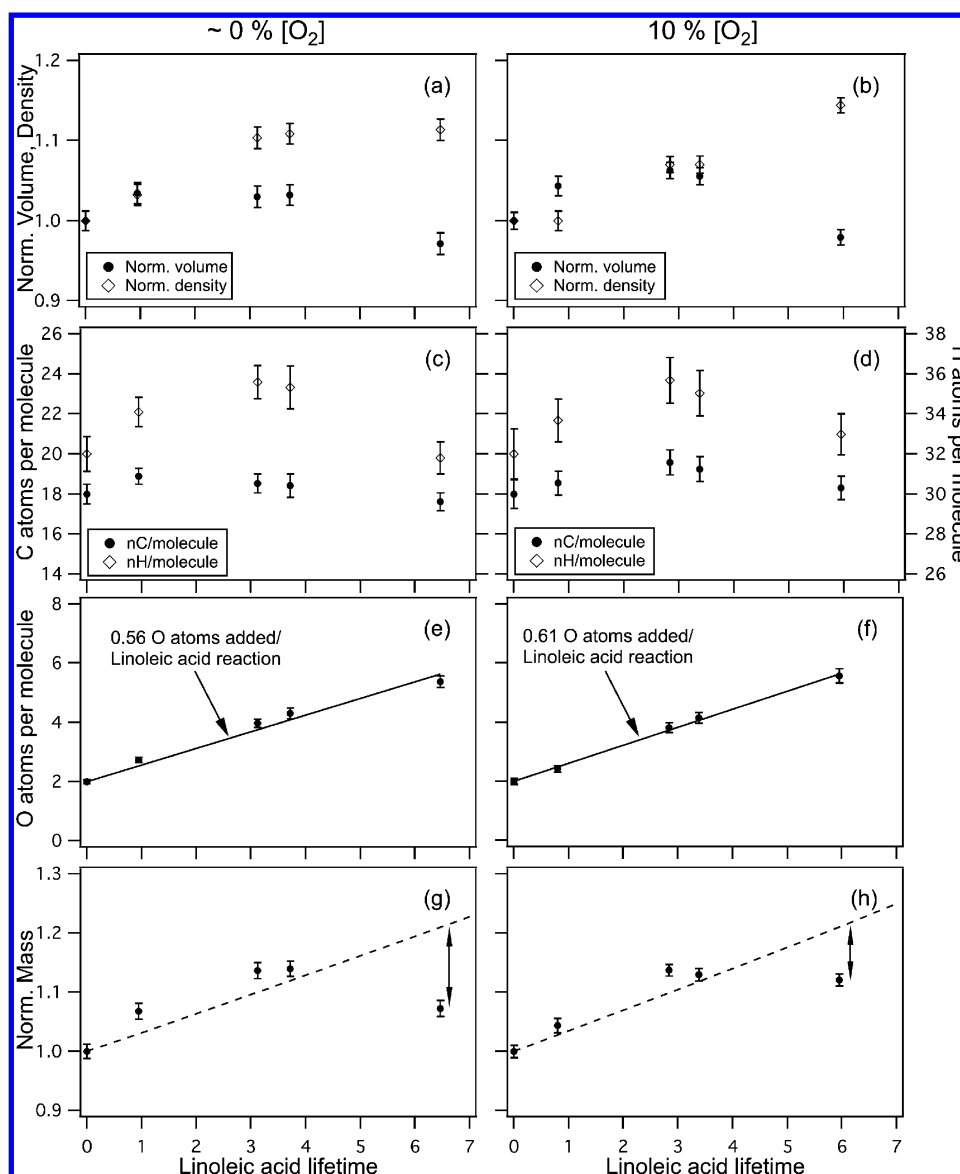
Figure 8. Elemental analysis of linoleic acid particles as a function of linoleic acid lifetime at $[H_2O_2]$ = 20.7 ppm for (a, c, e, and g) $[O_2]$ = ∼ 0% and (b, d, f, and h) $[O_2]$ = 10%. Panels (a) and (b): particle volume and density (normalized to the initial volume and density per unreacted particle). Panels (c) and (d): average number of C and H atoms per linoleic acid molecule. Panels (e) and (f): average number of O atoms per linoleic acid molecule. Panels (g) and (h): aerosol mass (normalized to the initial mass per unreacted particle). In panels (e) and (f), the measured number of O atoms per linoleic acid molecule is fit using the linear function $2 + mx$ (solid lines) where m is slope. In panels (g) and (h), the measured particle mass data is compared with the particle mass predictions (dashed lines) based on the assumption that an average of 0.56 and 0.61 O atoms are added per reactive loss of linoleic acid at ∼0% and 10% $[O_2]$, respectively. The degree of particle volatilization is the difference between the measured particle mass and the predicted mass (arrows).

particle volatilization occurs at lifetimes ≥3 in the OH + squalane (alkane equivalent of squalene) reaction.[17,27] Since particle volatilization occurs at much earlier lifetimes in the OH + squalene reaction, this indicates that fragmentation is potentially an important pathway in the oxidation of branched unsaturated organic aerosol.

The mass and elemental composition measurements of squalene particles are compared to the measurements of linoleic acid particles. Figure 8 shows the mass measurements and elemental analysis of linoleic acid particles as a function of linoleic acid lifetime at 20.7 ppm $[H_2O_2]$ for ∼0 and 10% $[O_2]$. Parts a and b of Figure 8 show that, at both ∼0 and 10% $[O_2]$, particle volume increases slightly before decreasing. The

particle density increases with oxidation at both ∼0 and 10% $[O_2]$.

While O_2 appears to influence the oxidative evolution of the squalene particle mass and elemental content, the influence of O_2 on the oxidative transformation of linoleic acid particles is less apparent. Parts c and d of Figure 8 show that, at both ∼0 and 10% $[O_2]$, the average number of C atoms in the linoleic acid molecule stays roughly constant at 18 (within experimental error) during oxidation. Additionally, at both ∼0 and 10% $[O_2]$, the average number of H atoms in the linoleic acid molecule increases at early linoleic acid lifetimes (0 to ∼3 linoleic acid lifetimes) before decreasing. Parts e and f of Figure 8 show that the average number of O atoms in the linoleic acid molecule increases linearly at approximately the same rate for both ∼0

and 10% $[O_2]$ (0.56 ± 0.03 and 0.61 ± 0.01 O atoms are added per reactive loss of linoleic acid, respectively). The origin of the difference between the average number of O atoms added to the linoleic acid and squalene molecules is not clear, but it may be attributed to different branching ratios for secondary chain reactions present in the two systems.

The linoleic acid particle mass measurements are compared with mass predictions (shown as dashed lines in Figure 8g and h) based on measurements that an average of 0.56 and 0.61 O atoms are added per reactive loss of linoleic acid at ∼0 and 10% $[O_2]$, respectively. Parts g and h of Figure 8 show that, at both ∼0 and 10% $[O_2]$, the measured particle mass and predicted particle mass are roughly similar from 0 to ∼3.5 linoleic acid lifetimes. In both cases, the measured particle mass starts to decrease after ∼3.5 linoleic acid lifetime and deviates from the predicted mass. This indicates that, at both ∼0 and 10% $[O_2]$, functionalization dominates the reaction during the early stages of oxidation, while fragmentation increases in importance as the particle becomes more oxidized.

Since the oxidative transformation of the linoleic acid particle mass and elemental content appear to be similar at ∼0 and 10% $[O_2]$, this suggests that O_2 does not substantially influence the relative importance of functionalization and fragmentation reactions in the OH + linoleic acid reaction. This is in contrast to the OH + squalene reaction where O_2 clearly appears to promote fragmentation reactions. This implies that while fragmentation becomes an important reaction channel when O_2 is present in the OH oxidation of branched unsaturated organic aerosol (i.e., squalene), O_2 does not appear to alter the relative importance of fragmentation reactions in the OH oxidation of linear unsaturated organic aerosol (i.e., linoleic acid). The role of O_2 in the OH + squalene and OH + linoleic acid reactions will be discussed further in section 4.

4. DISCUSSION: OH + SQUALENE VS OH + UNSATURATED FATTY ACID

The value of γ_{eff}^{Sqe} measured at 10% $[O_2]$ and 18.5 ppm $[H_2O_2]$ is 2.34 ± 0.07, while the effective uptake coefficients for the unsaturated fatty acids (γ_{eff}^{UFA}) measured previously at 10% $[O_2]$ and 20.7 ppm $[H_2O_2]$ are 1.72 ± 0.08 for oleic acid (OA), 3.75 ± 0.18 for linoleic acid (LA), and 5.73 ± 0.14 for linolenic acid (LNA).[21] These values indicate that the oxidation rate of squalene particles is slower than that of linoleic acid and linolenic acid particles. These results are surprising since squalene might be expected to react faster than the unsaturated fatty acids due to the larger number of C=C double bonds available for radical addition and subsequent secondary chain chemistry. From SAR[11] calculations, it is expected that, in the absence of secondary chain chemistry, OH radicals would react with squalene ∼7 times faster than oleic acid, ∼4 times faster than linoleic acid, and ∼3 times faster than linolenic acid.

The higher oxidation rate of unsaturated fatty acid particles (i.e., linoleic acid and linolenic acid) relative to squalene particles may be explained by the reactive uptake of OH radicals at the surface of these particles (γ_{OH}). The γ_{OH} values measured by Waring et al.[41] from the reactive loss of gas-phase OH radicals onto squalene and oleic acid surfaces are 0.39 ± 0.07 and 0.24 ± 0.10, respectively. These measurements suggest that the OH heterogeneous reactive uptake at the squalene surface may only be ∼1.6 times larger than the reactive uptake at the oleic acid surface, rather than ∼7 times larger as predicted by SAR[11] calculations. This suggests that other factors (e.g., molecular orientation at the particle surface)

may play a bigger role in the aerosol reactivity than simply the number of C=C double bonds.

The more rapid oxidation of unsaturated fatty acid particles (i.e., linoleic acid and linolenic acid) relative to squalene particles may originate, in part, from differences in the molecular orientation of squalene and unsaturated fatty acid molecules at the particle surface. Hearn et al.[46] reported that oleic acid particles reacted with O_3 at a faster rate than methyl oleate due to differences in the molecular orientation at the particle surface. X-ray diffraction studies on liquid oleic acid[47,48] showed that the acid molecules exist primarily as dimers through hydrogen bonding of the carbonyl oxygen and the acidic hydrogen. The carboxylic acid groups of one dimer and the terminal methyl groups of another dimer align alternatively in the same lateral plane within the liquid. Hearn et al.[46] postulate that oleic acid molecules are similarly orderly arranged at the particle surface, leading to an increase in the density of C=C double bonds at the particle surface, and consequently a fast surface reaction between O_3 and a C=C double bond. In contrast, methyl oleate molecules are expected to be isotropically oriented within the particle, since they do not participate in hydrogen bonding. This results in a slower reaction, since the C=C double bonds of methyl oleate molecules are not as accessible to O_3 at the particle surface (relative to oleic acid). In the OH + unsaturated fatty acid reaction, it is possible that the proposed ordered arrangement of unsaturated fatty acid molecules at the particle surface[46] similarly increases the overall probability of a surface OH reaction with a C=C double bond. Molecular dynamics simulations of liquid squalene show that squalene molecules are isotropically oriented at the liquid surface.[49] Analogous to the O_3 + methyl oleate reaction,[46] this arrangement of squalene molecules within the particle may reduce the overall probability of a surface OH reaction with a C=C double bond.

The more rapid oxidation of unsaturated fatty acid particles could also be attributed to differences in particle-phase secondary chain chemistry. The rate coefficients of secondary chain reactions that consume squalene molecules in the OH + squalene reaction may be smaller than the rate coefficients of secondary chain reactions that consume unsaturated fatty acid molecules in the OH + unsaturated fatty acid reactions. Studies have shown that gas-phase unsaturated oxygenated organics (e.g., acids, alcohols, ketones) are more reactive toward OH radicals than their alkene equivalents due to the formation of a hydrogen-bonded complex (via interactions between the OH radical and the oxygenated functional group of the molecule) that promotes the formation of stable reaction products.[50−54] Here it is possible that the presence of a carboxylic acid functional group in the unsaturated fatty acids enhances particle-phase chain cycling reactions, which leads to a higher oxidation rate for the unsaturated fatty acid particles.

One other difference between the OH + squalene and OH + unsaturated fatty acid reactions is the role of O_2 in the two systems. Figure 6a shows that γ_{eff}^{Sqe} increases with increasing $[O_2]$, thus implying that O_2 promotes chain propagation in the OH + squalene reaction. Elemental analysis of squalene particles (shown in Figure 7) shows that the particle mass decreases by a greater extent during oxidation at 10% $[O_2]$ compared to oxidation at ∼0% $[O_2]$. In contrast, the values of γ_{eff}^{Sqe} decrease with increasing $[O_2]$,[21] indicating that O_2 promotes chain termination in the OH + unsaturated fatty acid reactions. Elemental analysis of linoleic acid particles (shown in Figure 8) also shows that the evolution of particle

mass and elemental content (particulate C, H, and O atoms) is approximately similar during oxidation at ~0 and 10% $[O_2]$.

These differences in the role of O_2 in the two systems can be attributed to differences in the molecular structures of squalene and the unsaturated fatty acids. Squalene is a branched alkene with six C=C double bonds. Previous studies suggest that OH adds preferentially to the less substituted carbon of the C=C double bond (to form tertiary hydroxyalkyl radicals) as opposed to the more substituted carbon of the C=C double bond.[12,55] Therefore, tertiary hydroxyperoxy radicals will be formed in high yields (relative to secondary hydroxyperoxy radicals) when O_2 is present in the reaction. The formation of terminal oxygenated products (R5 in Figure 4) is potentially suppressed in the reaction between two tertiary hydroxyperoxy radicals due to the lack of H atoms adjacent to the peroxy radical. Instead, tertiary hydroxyalkoxy radicals are likely the dominant products from the reaction between two tertiary hydroxyperoxy radicals (R6 in Figure 4). These tertiary hydroxyalkoxy radicals can dissociate to form lower molecular weight products (R7 in Figure 4), which may evaporate from the particle, resulting in a detectable loss of particle mass (i.e., particle volatilization). The observation of significant particle volatilization at 10% $[O_2]$ (shown in Figure 7h) suggests that tertiary hydroxyalkoxy radicals are an important radical intermediate when O_2 is present in the reaction.

The importance of the tertiary hydroxyalkoxy radical intermediate is also evident in Figure 6a, which shows that γ_{eff}^{Sqe} increases with increasing $[O_2]$. Based on the general reaction scheme shown in Figure 4, pathways R2 and R8 are chain propagation reactions that accelerate the reactive depletion of squalene molecules when O_2 is present in the reaction. When O_2 is absent, pathway R2 becomes the sole chain propagation channel since hydroxyperoxy radicals are not formed. Therefore, the radical chain chemistry in the particle is arrested with decreasing $[O_2]$, causing γ_{eff}^{Sqe} to decrease when $[O_2]$ is decreased.

In contrast to squalene, the unsaturated fatty acids are linear molecules. OH addition is predicted to be approximately equally rapid at the two carbons in the C=C double bonds.[12,55] Therefore, secondary hydroxyperoxy radicals are expected to be formed in high yields when O_2 is present in the reaction. As shown in our group's previous study of the OH + unsaturated fatty acid reactions,[21] secondary hydroxyalkyl radicals propagate the particle-phase secondary chain chemistry in the absence of O_2 by reacting with unsaturated fatty acid molecules (R2 in Figure 4). When increasing amounts of O_2 are added to the reaction, the secondary hydroxyalkyl radicals can react with O_2 instead to form secondary hydroxyperoxy radicals (R4 in Figure 4). These secondary hydroxyperoxy radicals (which have H atoms adjacent to the peroxy radical) can then react with each other via the Russell and Bennett–Summers mechanisms[37–40] (R5 in Figure 4) to form terminal oxygenated products (i.e., chain termination). This slows the radical chain chemistry in the particle, causing γ_{eff}^{UFA} to decrease with increasing $[O_2]$.

Elemental analysis of linoleic acid particles suggests that the formation of secondary hydroxyalkoxy radicals (R6 in Figure 4) is a minor channel in the OH + unsaturated fatty acid reactions. If secondary hydroxyalkoxy radicals were formed in high yields when O_2 is present in the reaction, one might expect the average number of C atoms in the linoleic acid molecule and the particle mass to decrease significantly at 10% $[O_2]$ (relative to at ~0% $[O_2]$) since a fraction of these hydroxyalkoxy radicals

could dissociate and form volatile lower molecular weight products that may evaporate from the particle (R7 in Figure 4). However, Figure 8 shows that the average number of C atoms in the linoleic acid molecule stays constant at 18 (within experimental error) during oxidation at 10% $[O_2]$ and the evolution of the particle mass is similar at ~0 and 10% $[O_2]$. These measurements suggest that the formation of secondary hydroxyalkoxy radicals is a minor channel in the hydroxyperoxy self-reaction, and the formation of terminal oxygenated products (e.g., diols and hydroxycarbonyls) is the dominant channel when O_2 is present in the reaction. This is consistent with a study of the NO_3-initiated oxidation of oleic acid particles,[29] which found that the formation of oxygenated products is a major reaction pathway while the formation of alkoxy radicals (which can fragment) is of minimal importance.

5. CONCLUSIONS

Two model reaction systems, OH + squalene and OH + unsaturated fatty acid (oleic acid, linoleic acid, and linolenic acid), are analyzed to investigate the effect of molecular structure (branched vs linear) and chemical functionality (alkene vs carboxylic acid) on the reaction rates and mechanism in the OH-initiated oxidation of unsaturated organic particles. The value of γ_{eff}^{Sqe} measured at 10% $[O_2]$ and 18.5 ppm $[H_2O_2]$ is 2.34 ± 0.07, while the values of γ_{eff}^{UFA} measured previously for oleic acid, linoleic acid, and linolenic acid at 10% $[O_2]$ and 20.7 ppm $[H_2O_2]$ are 1.72 ± 0.08, 3.75 ± 0.18, and 5.73 ± 0.14, respectively. Since γ_{eff}^{Sqe} and γ_{eff}^{UFA} are larger than one, there is clear evidence for particle-phase secondary chain chemistry.

γ_{eff}^{Sqe} is smaller than γ_{eff}^{LA} and γ_{eff}^{LNA} even though squalene has more C=C double bonds than linoleic acid and linolenic acid. This may be attributed to differences in the reactive uptakes of OH radicals at the particle surface and particle-phase secondary reactions in the two systems. γ_{eff}^{Sqe} increases with $[O_2]$ in the reactor, while the values of γ_{eff}^{UFA} decrease with increasing $[O_2]$. This suggests that O_2 promotes chain propagation in the OH + squalene reaction and promotes chain termination in the OH + unsaturated fatty acid reactions. The values of γ_{eff}^{Sqe} and γ_{eff}^{UFA} decrease when the absolute $[OH]$ in the flow reactor is increased. This inverse relationship between the effective uptake coefficient and $[OH]$ is attributed to the competing rates of chain propagation and termination reactions.

Elemental analysis of squalene particles shows that, while particle volatilization only becomes important in the later stages of oxidation at ~0% $[O_2]$, significant particle volatilization occurs once oxidation is initiated at 10% $[O_2]$. In contrast, elemental analysis of linoleic acid particles shows that $[O_2]$ does not influence the rate of particle volatilization in the OH + linoleic acid reaction. Together these measurements suggest that fragmentation reactions are important when O_2 is present in the OH oxidation of branched unsaturated organic aerosol, while O_2 does not alter the relative importance of fragmentation reactions in the OH oxidation of linear unsaturated organic aerosol.

■ AUTHOR INFORMATION

Corresponding Author
*E-mail: krwilson@lbl.gov, 510-495-2474.

Notes
The authors declare no competing financial interest.

4117

dx.doi.org/10.1021/jp502666g | J. Phys. Chem. A 2014, 118, 4106–4119

■ REFERENCES

(1) Finlayson-Pitts, B. J.; Pitts, J. N. *Chemistry of the Upper and Lower Atmosphere: Theory, Experiments, and Applications*; Academic Press: San Diego, 2000.

(2) Hallquist, M.; Wenger, J. C.; Baltensperger, U.; Rudich, Y.; Simpson, D.; Claeys, M.; Dommen, J.; Donahue, N. M.; George, C.; Goldstein, A. H.; et al. The Formation, Properties and Impact of Secondary Organic Aerosol: Current and Emerging Issues. *Atmos. Chem. Phys.* **2009**, *9*, 5155−5236.

(3) Rudich, Y. Laboratory Perspectives on the Chemical Transformations of Organic Matter in Atmospheric Particles. *Chem. Rev.* **2003**, *103*, 5097−5124.

(4) Jimenez, J. L.; Canagaratna, M. R.; Donahue, N. M.; Prevot, A. S. H.; Zhang, Q.; Kroll, J. H.; DeCarlo, P. F.; Allan, J. D.; Coe, H.; Ng, N. L.; et al. Evolution of Organic Aerosols in the Atmosphere. *Science* **2009**, *326*, 1525−1529.

(5) Ng, N. L.; Canagaratna, M. R.; Zhang, Q.; Jimenez, J. L.; Tian, J.; Ulbrich, I. M.; Kroll, J. H.; Docherty, K. S.; Chhabra, P. S.; Bahreini, R.; et al. Organic Aerosol Components Observed in Northern Hemispheric Datasets from Aerosol Mass Spectrometry. *Atmos. Chem. Phys.* **2010**, *10*, 4625−4641.

(6) Robinson, A. L.; Donahue, N. M.; Rogge, W. F. Photochemical Oxidation and Changes in Molecular Composition of Organic Aerosol in the Regional Context. *J. Geophys. Res, D: Atmos.* **2006**, *111*, D03302.

(7) Atkinson, R. Gas-Phase Tropospheric Chemistry of Organic-Compounds. *J. Phys. Chem. Ref. Data* **1994**, R1−R216.

(8) Atkinson, R. Gas-Phase Tropospheric Chemistry of Volatile Organic Compounds 0.1. Alkanes and Alkenes. *J. Phys. Chem. Ref. Data* **1997**, *26*, 215−290.

(9) Atkinson, R. Kinetics of the Gas-Phase Reactions of OH Radicals with Alkanes and Cycloalkanes. *Atmos. Chem. Phys.* **2003**, *3*, 2233−2307.

(10) Atkinson, R.; Arey, J. Atmospheric Degradation of Volatile Organic Compounds. *Chem. Rev.* **2003**, *103*, 4605−4638.

(11) Kwok, E. S. C.; Atkinson, R. Estimation of Hydroxyl Radical Reaction-Rate Constants for Gas-Phase Organic-Compounds Using a Structure-Reactivity Relationship—An Update. *Atmos. Environ.* **1995**, *29*, 1685−1695.

(12) Peeters, J.; Boullart, W.; Pultau, V.; Vandenberk, S.; Vereecken, L. Structure−Activity Relationship for the Addition of OH to (Poly)Alkenes: Site-Specific and Total Rate Constants. *J. Phys. Chem. A* **2007**, *111*, 1618−1631.

(13) Moise, T.; Rudich, Y. Uptake of Cl and Br by Organic—A Perspective on Organic Aerosols Processing by Tropospheric Oxidants. *Geophys. Res. Lett.* **2001**, *28*, 4083−4086.

(14) Liu, C. L.; Smith, J. D.; Che, D. L.; Ahmed, M.; Leone, S. R.; Wilson, K. R. The Direct Observation of Secondary Radical Chain Chemistry in the Heterogeneous Reaction of Chlorine Atoms with Submicron Squalane Droplets. *Phys. Chem. Chem. Phys.* **2011**, *13*, 8993−9007.

(15) Ruehl, C. R.; Nah, T.; Isaacman, G.; Worton, D. R.; Chan, A. W. H.; Kolesar, K. R.; Cappa, C. D.; Goldstein, A. H.; Wilson, K. R. The Influence of Molecular Structure and Aerosol Phase on the Heterogeneous Oxidation of Normal and Branched Alkanes by OH. *J. Phys. Chem. A* **2013**, *117*, 3990−4000.

(16) Kroll, J. H.; Donahue, N. M.; Jimenez, J. L.; Kessler, S. H.; Canagaratna, M. R.; Wilson, K. R.; Altieri, K. E.; Mazzoleni, L. R.; Wozniak, A. S.; Bluhm, H.; et al. Carbon Oxidation State as a Metric for Describing the Chemistry of Atmospheric Organic Aerosol. *Nat. Chem.* **2011**, *3*, 133−139.

(17) Kroll, J. H.; Smith, J. D.; Che, D. L.; Kessler, S. H.; Worsnop, D. R.; Wilson, K. R. Measurement of Fragmentation and Functionalization Pathways in the Heterogeneous Oxidation of Oxidized Organic Aerosol. *Phys. Chem. Chem. Phys.* **2009**, *11*, 8005−8014.

(18) Wilson, K. R.; Smith, J. D.; Kessler, S. H.; Kroll, J. H. The Statistical Evolution of Multiple Generations of Oxidation Products in the Photochemical Aging of Chemically Reduced Organic Aerosol. *Phys. Chem. Chem. Phys.* **2012**, *14*, 1468−1479.

(19) Kessler, S. H.; Smith, J. D.; Che, D. L.; Worsnop, D. R.; Wilson, K. R.; Kroll, J. H. Chemical Sinks of Organic Aerosol: Kinetics and Products of the Heterogeneous Oxidation of Erythritol and Levoglucosan. *Environ. Sci. Technol.* **2010**, *44*, 7005−7010.

(20) Isaacman, G.; Chan, A. W. H.; Nah, T.; Worton, D. R.; Ruehl, C. R.; Wilson, K. R.; Goldstein, A. H. Heterogeneous OH Oxidation of Motor Oil Particles Causes Selective Depletion of Branched and Less Cyclic Hydrocarbons. *Environ. Sci. Technol.* **2012**, *46*, 10632−10640.

(21) Nah, T.; Kessler, S. H.; Daumit, K. E.; Kroll, J. H.; Leone, S. R.; Wilson, K. R. OH-Initiated Oxidation of Sub-Micron Unsaturated Fatty Acid Particles. *Phys. Chem. Chem. Phys.* **2013**, *15*, 18649−18663.

(22) Gloaguen, E.; Mysak, E. R.; Leone, S. R.; Ahmed, M.; Wilson, K. R. Investigating the Chemical Composition of Mixed Organic-Inorganic Particles by "Soft" Vacuum Ultraviolet Photoionization: The Reaction of Ozone with Anthracene on Sodium Chloride Particles. *Int. J. Mass Spectrom.* **2006**, *258*, 74−85.

(23) Aiken, A. C.; DeCarlo, P. F.; Jimenez, J. L. Elemental Analysis of Organic Species with Electron Ionization High-Resolution Mass Spectrometry. *Anal. Chem.* **2007**, *79*, 8350−8358.

(24) Aiken, A. C.; Decarlo, P. F.; Kroll, J. H.; Worsnop, D. R.; Huffman, J. A.; Docherty, K. S.; Ulbrich, I. M.; Mohr, C.; Kimmel, J. R.; Sueper, D.; et al. O/C and Om/Oc Ratios of Primary, Secondary, and Ambient Organic Aerosols with High-Resolution Time-of-Flight Aerosol Mass Spectrometry. *Environ. Sci. Technol.* **2008**, *42*, 4478−4485.

(25) DeCarlo, P. F.; Kimmel, J. R.; Trimborn, A.; Northway, M. J.; Jayne, J. T.; Aiken, A. C.; Gonin, M.; Fuhrer, K.; Horvath, T.; Docherty, K. S.; et al. Field-Deployable, High-Resolution, Time-of-Flight Aerosol Mass Spectrometer. *Anal. Chem.* **2006**, *78*, 8281−8289.

(26) Jayne, J. T.; Leard, D. C.; Zhang, X. F.; Davidovits, P.; Smith, K. A.; Kolb, C. E.; Worsnop, D. R. Development of an Aerosol Mass Spectrometer for Size and Composition Analysis of Submicron Particles. *Aerosol Sci. Technol.* **2000**, *33*, 49−70.

(27) Smith, J. D.; Kroll, J. H.; Cappa, C. D.; Che, D. L.; Liu, C. L.; Ahmed, M.; Leone, S. R.; Worsnop, D. R.; Wilson, K. R. The Heterogeneous Reaction of Hydroxyl Radicals with Sub-Micron Squalane Particles: A Model System for Understanding the Oxidative Aging of Ambient Aerosols. *Atmos. Chem. Phys.* **2009**, *9*, 3209−3222.

(28) Hearn, J. D.; Smith, G. D.; Mixed-Phase, A. Relative Rates Technique for Measuring Aerosol Reaction Kinetics. *Geophys. Res. Lett.* **2006**, *33*, L17895.

(29) Docherty, K. S.; Ziemann, P. J. Reaction of Oleic Acid Particles with NO₃ Radicals: Products, Mechanism, and Implications for Radical-Initiated Organic Aerosol Oxidation. *J. Phys. Chem. A* **2006**, *110*, 3567−3577.

(30) George, I. J.; Abbatt, J. P. D. Heterogeneous Oxidation of Atmospheric Aerosol Particles by Gas-Phase Radicals. *Nat. Chem.* **2010**, *2*, 713−722.

(31) George, I. J.; Vlasenko, A.; Slowik, J. G.; Broekhuizen, K.; Abbatt, J. P. D. Heterogeneous Oxidation of Saturated Organic Aerosols by Hydroxyl Radicals: Uptake Kinetics, Condensed-Phase Products, and Particle Size Change. *Atmos. Chem. Phys.* **2007**, *7*, 4187−4201.

(32) McNeill, V. F.; Yatavelli, R. L. N.; Thornton, J. A.; Stipe, C. B.; Landgrebe, O. Heterogeneous OH Oxidation of Palmitic Acid in Single Component and Internally Mixed Aerosol Particles: Vaporization and the Role of Particle Phase. *Atmos. Chem. Phys.* **2008**, *8*, 5465−5476.

4118

dx.doi.org/10.1021/jp502666g | *J. Phys. Chem. A* 2014, 118, 4106−4119

(33) Atkinson, R.; Tuazon, E. C.; Aschmann, S. M. Products of the Gas-Phase Reaction of the OH Radical with 3-Methyl-1-Butene in the Presence of NO. *Int. J. Chem. Kinet.* **1998**, *30*, 577−587.

(34) Atkinson, R.; Tuazon, E. C.; Carter, W. P. L. Extent of H-Atom Abstraction from the Reaction of the OH Radical with 1-Butene under Atmospheric Conditions. *Int. J. Chem. Kinet.* **1985**, *17*, 725−734.

(35) D'andrea, T. M.; Zhang, X.; Jochnowitz, E. B.; Lindeman, T. G.; Simpson, C. J. S. M.; David, D. E.; Curtiss, T. J.; Morris, J. R.; Ellison, G. B. Oxidation of Organic Films by Beams of Hydroxyl Radicals. *J. Phys. Chem. B* **2008**, *112*, 535−544.

(36) Moussa, S. G.; Finlayson-Pitts, B. J. Reaction of Gas Phase OH with Unsaturated Self-Assembled Monolayers and Relevance to Atmospheric Organic Oxidations. *Phys. Chem. Chem. Phys.* **2010**, *12*, 9419−9428.

(37) Hearn, J. D.; Renbaum, L. H.; Wang, X.; Smith, G. D. Kinetics and Products from Reaction of Cl Radicals with Dioctyl Sebacate (Dos) Particles in O$_2$: A Model for Radical-Initiated Oxidation of Organic Aerosols. *Phys. Chem. Chem. Phys.* **2007**, *9*, 4803−4813.

(38) Ingold, K. U. Peroxy Radicals. *Acc. Chem. Res.* **1969**, *2*, 1−9.

(39) von Sonntag, C.; Dowideit, P.; Fang, X. W.; Mertens, R.; Pan, X. M.; Schuchmann, M. N.; Schuchmann, H. P. The Fate of Peroxyl Radicals in Aqueous Solution. *Water Sci. Technol.* **1997**, *35*, 9−15.

(40) von Sonntag, C.; Schuchmann, H. P. The Elucidation of Peroxyl Radical Reactions in Aqueous Solution with the Help of Radiation-Chemical Methods. *Angew. Chem., Int. Ed. Engl.* **1991**, *30*, 1229−1253.

(41) Waring, C.; King, K. L.; Bagot, P. A. J.; Costen, M. L.; McKendrick, K. G. Collision Dynamics and Reactive Uptake of Oh Radicals at Liquid Surfaces of Atmospheric Interest. *Phys. Chem. Chem. Phys.* **2011**, *13*, 8457−8469.

(42) Lide, D. R. *CRC Handbook of Chemistry and Physics*, 85th ed.; CRC Press Inc LLC: 2004.

(43) Tesa-Serrate, M. A.; King, K. L.; Paterson, G.; Costen, M. L.; McKendrick, K. G. Site and Bond-Specific Dynamics of Reactions at the Gas-Liquid Interface. *Phys. Chem. Chem. Phys.* **2014**, *16*, 173−183.

(44) Renbaum, L. H.; Smith, G. D. Artifacts in Measuring Aerosol Uptake Kinetics: The Roles of Time, Concentration and Adsorption. *Atmos. Chem. Phys.* **2011**, *11*, 6881−6893.

(45) DeCarlo, P. F.; Slowik, J. G.; Worsnop, D. R.; Davidovits, P.; Jimenez, J. L. Particle Morphology and Density Characterization by Combined Mobility and Aerodynamic Diameter Measurements. Part 1: Theory. *Aerosol Sci. Technol.* **2004**, *38*, 1185−1205.

(46) Hearn, J. D.; Lovett, A. J.; Smith, G. D. Ozonolysis of Oleic Acid Particles: Evidence for a Surface Reaction and Secondary Reactions Involving Criegee Intermediates. *Phys. Chem. Chem. Phys.* **2005**, *7*, 501−511.

(47) Iwahashi, M.; Kasahara, Y. Dynamic Molecular Movements and Aggregation Structures of Lipids in a Liquid State. *Curr. Opin. Colloid Interface Sci.* **2011**, *16*, 359−366.

(48) Iwahashi, M.; Kasahara, Y.; Matsuzawa, H.; Yagi, K.; Nomura, K.; Terauchi, H.; Ozaki, Y.; Suzuki, M. Self-Diffusion, Dynamical Molecular Conformation, and Liquid Structures of N-Saturated and Unsaturated Fatty Acids. *J. Phys. Chem. B* **2000**, *104*, 6186−6194.

(49) King, K. L.; Paterson, G.; Rossi, G. E.; Iljina, M.; Westacott, R. E.; Costen, M. L.; McKendrick, K. G. Inelastic Scattering of OH Radicals from Organic Liquids: Isolating the Thermal Desorption Channel. *Phys. Chem. Chem. Phys.* **2013**, *15*, 12852−12863.

(50) Banco, M. B.; Barnes, I.; Wiesen, P. Kinetic Investigation of the OH Radical and Cl Atom Initiated Degradation of Unsaturated Ketones at Atmospheric Pressure and 298 K. *J. Phys. Chem. A* **2012**, *116*, 6033−6040.

(51) Smith, I. W. M.; Ravishankara, A. R. Role of Hydrogen-Bonded Intermediates in the Bimolecular Reactions of the Hydroxyl Radical. *J. Phys. Chem. A* **2002**, *106*, 4798−4807.

(52) Mellouki, A.; Le Bras, G.; Sidebottom, H. Kinetics and Mechanisms of the Oxidation of Oxygenated Organic Compounds in the Gas Phase. *Chem. Rev.* **2003**, *103*, 5077−5096.

(53) Orlando, J. J.; Tyndall, G. S.; Ceazan, N. Rate Coefficients and Product Yields from Reaction of Oh with 1-Penten-3-ol, (Z)-2-Penten-1-ol, and Allyl Alcohol (2-Propen-1-ol). *J. Phys. Chem. A* **2001**, *105*, 3564−3569.

(54) Papagni, C.; Arey, J.; Atkinson, R. Rate Constants for the Gas-Phase Reactions of Oh Radicals with a Series of Unsaturated Alcohols. *Int. J. Chem. Kinet.* **2001**, *33*, 142−147.

(55) Ziemann, P. J. Effects of Molecular Structure on the Chemistry of Aerosol Formation from the Oh-Radical-Initiated Oxidation of Alkanes and Alkenes. *Int. Rev. Phys. Chem.* **2011**, *30*, 161−195.